Journal of Photochemistry and Photobiology A: Chemistry 199 (2008) 57–63

Contents lists available at ScienceDirect

Journal of Photochemistry and Photobiology A: Chemistry

journal homepage: www.elsevier.com/locate/jphotochem

Ternary lanthanide (Er^{3+}, Nd^{3+}, Yb^{3+}, Sm^{3+}, Pr^{3+}) complex-functionalized mesoporous SBA-15 materials that emit in the near-infrared range

Li-Ning Sun[a,b], Yu Zhang[a], Jiang-Bo Yu[a], Chun-Yun Peng[a], Hong-Jie Zhang[a,*]

[a] State Key Laboratory of Rare Earth Resource Utilizations, Changchun Institute of Applied Chemistry, Chinese Academy of Sciences, 5625 Renmin Street, Changchun 130022, PR China
[b] Graduate School of the Chinese Academy of Sciences, Beijing, PR China

ARTICLE INFO

Article history:
Received 21 January 2008
Received in revised form 8 April 2008
Accepted 26 April 2008
Available online 3 May 2008

Keywords:
NIR luminescence
SBA-15
Covalently linked
Ternary lanthanide complex
β-Diketone

ABSTRACT

The ternary lanthanide complexes [Ln(hfth)$_3$phen] (Ln = Er, Nd, Yb, Sm) and [Pr(tfnb)$_3$phen] have been successfully covalently attached in the ordered SBA-15 mesoporous materials via a functionalized 1,10-phenanthroline group 5-(*N*,*N*-bis-3-(triethoxysilyl)propyl)ureyl-1,10-phenanthroline (Phen-Si). The derivative materials [denoted as Ln(hfth)$_3$phen–S15 and Pr(tfnb)$_3$phen–S15; Ln = Er, Yb, Nd, Sm; hfth = 4,4,5,5,6,6,6-heptafluoro-1-(2-thienyl)hexane-1,3-dionate; tfnb = 4,4,4-trifluoro-1-(2-naphthyl)-1,3-butanedionate] were characterized by powder X-ray diffraction (XRD), transmission electron microscopy (TEM), and N_2 adsorption/desorption. The fluorescence spectra and luminescence lifetimes of these lanthanide-complex-functionalized materials were also recorded. After ligand-mediated excitation, the emission spectra of the Ln(hfth)$_3$phen–S15 and Pr(tfnb)$_3$phen–S15 materials all display the characteristic NIR luminescence of the corresponding lanthanide ions through the intramolecular energy transfer from the ligands to the lanthanide ions. With these lanthanide-complex-functionalized materials, the luminescent spectral region from 1300 to 1600 nm, which is of particular interest for telecommunication applications, can be covered completely.

1. Introduction

Lanthanide complexes, especially Eu(III) and Tb(III) complexes, have attracted much attention for their unique luminescent properties in the visible region for application in organic light-emitting diodes (OLED) [1,2]. Recently, the lanthanide ions that are emissive in the near-infrared region (NIR) of the spectrum (800–1700 nm), such as Er(III), Nd(III), Yb(III), Pr(III), and Sm(III), have received increasing attention for their potential applications in the optical telecommunication [3,4], laser systems [5], and medical diagnosis [6]. The design of sensitizer-functionalized lanthanide complexes that exhibit efficient luminescence in the NIR region is currently of interest and much effort has been directed toward investigating ligands for efficient sensitization of the NIR-emitting lanthanides [7,8]. It has been reported that the NIR-emitting lanthanide ions are particularly prone to vibrational deactivation [9]. However, ligands and coordinated solvent molecules usually contain C–H and O–H bonds that can cause vibrational quenching of the excited ions, leading to the lower NIR-luminescent intensities. It is well known that deuteration or fluorination of hydrogen-containing ligands, together with exclusion of coordinated water, can extend the lifetime of NIR luminescence and improve the luminescence intensity from lanthanide complexes [10].

However, due to the low photo- and thermal stability of the NIR-luminescent lanthanide complexes, for practical applications one of the strategies to improve the thermal stability, mechanical and light emission properties could be given by the incorporation of the samples into a rigid matrix [11]. Since the mesoporous silica materials were discovered in the early 1990s [12], the development of ordered mesoporous molecular sieves has been of widespread interest in material science. Mesostructured materials offer the rigidity and photostability, and at the same time have a well-defined hydrophilic/hydrophobic phase separation allowing for more sophisticated tuning of the lanthanide complex microenvironment. In addition, in our previous report, on the basis of certain conditions it was observed that the SBA-15-supported materials show an overall increase in relative lanthanide luminescent intensity and lifetime compared to the MCM-41-supported materials [13].

Herein, the syntheses of NIR-luminescent SBA-15 mesoporous materials attached with ternary lanthanide (Ln = Er, Nd, Yb, Sm, Pr) complexes by a functionalized 1,10-phenanthroline group 5-(*N*,*N*-bis-3-(triethoxysilyl)propyl)ureyl-1,10-phenanthroline (named as Phen-Si) have been reported. We selected two β-diketone

* Corresponding author. Tel.: +86 431 85262127; fax: +86 431 85698041.
E-mail address: hongjie@ciac.jl.cn (H.-J. Zhang).

1010-6030/$ – see front matter © 2008 Elsevier B.V. All rights reserved.
doi:10.1016/j.jphotochem.2008.04.015

ligands with polyfluorinated alkyl group, Hhfth and Htfnb (Hhfth = 4,4,5,5,6,6,6-heptafluoro-1-(2-thienyl)hexane-1,3-dione, Htfnb = 4,4,4-trifluoro-1-(2-naphthyl)-1,3-butanedione) to match with the 4f excited levels of the title lanthanide ions. Full characterization and detailed studies of NIR-luminescent properties of these mesoporous materials were investigated and discussed.

2. Experimental

2.1. Materials

Tetraethoxysilane (TEOS, Aldrich), 3-(triethoxysilyl)-propyl isocyanate (Aldrich), tri-block copolymer poly(ethylene glyco)-block-poly(propylene glycol)-block-poly(ethylene glycol) (Pluronic P123, $EO_{20}PO_{70}EO_{20}$, Aldrich), ethyl trifluoroacetate (Aldrich), fuming nitric acid, and ethanol were used as received. The solvent chloroform ($CHCl_3$) was used after desiccation with anhydrous calcium chloride. 1,10-Phenanthroline monohydrate (phen H_2O, 99%, AR) was bought from Beijing Fine Chemical Co. (Beijing, China). Ytterbium oxide (Yb_2O_3, 99.99%), neodymium oxide (Nd_2O_3, 99.99%), erbium oxide (Er_2O_3, 99.99%), samarium oxide (Sm_2O_3, 99.99%), and praseodymium oxide (Pr_6O_{11}, 99.99%) were purchased from Yue Long Chemical Plant (Shanghai, China). Hhfth and 2′-acetonaphthone were from Acros Organics Co. (Geel, Belgium). $LnCl_3$ (Ln = Er, Nd, Yb, Sm, Pr) were obtained by dissolving Ln_2O_3 (Ln = Er, Nd, Yb, Sm) and Pr_6O_{11} in concentrated hydrochloric acid (HCl) and removing the surplus HCl by evaporation.

2.2. Synthesis of phen-functionalized SBA-15 mesoporous material (phen–S15)

The starting reagent 5-amino-1,10-phenanthroline (named Phen-NH_2) was synthesized according to Ref. [14]. The modified phen group Phen-Si was prepared by the reaction of 3-(triethoxysilyl)-propyl isocyanate and Phen-NH_2 in $CHCl_3$ as described in the literature [15,16]. The phen–S15 was synthesized as described in our recent report [13]. The molar composition of the original synthetic mixture was Phen-Si:TEOS:P123:HCl:H_2O = 0.04:1.0:0.0172:6:208.33.

2.3. Synthesis of the [Ln(hfth)$_3$(H_2O)$_2$] complex (Ln = Er, Yb, Nd, Sm, Pr)

The synthesis procedure was according to the reported method [16]. The complexes obtained were dried overnight at 80 °C under vacuum.

2.4. Synthesis of the ligand Htfnb

The ligand Htfnb was synthesized by the reaction between 2-acetonaphthone and ethyl trifluoroacetate according to the procedure described in our previous report [17].

2.5. Synthesis of the [Pr(tfnb)$_3$(H_2O)$_2$] complex

The synthesis procedure for [Pr(tfnb)$_3$(H_2O)$_2$] was similar to that for [Ln(hfth)$_3$(H_2O)$_2$] complex except that $LnCl_3$ and Hhfth were replaced by $PrCl_3$ and Htfnb, respectively.

2.5.1. Elemental analysis

For [Er(hfth)$_3$(H_2O)$_2$], calculated: C, 30.88%; H, 1.38%. Found: C, 30.64%; H, 1.52%. For [Nd(hfth)$_3$(H_2O)$_2$], calculated: C, 31.50%; H, 1.41%. Found: C, 31.23%; H, 1.54%. For [Yb(hfth)$_3$(H_2O)$_2$], calculated: C, 30.73%; H, 1.38%. Found: C, 30.96%; H, 1.56%. For [Sm(hfth)$_3$(H_2O)$_2$], calculated: C, 31.33%; H, 1.40%. Found: C, 31.61%; H, 1.58%. For [Pr(hfth)$_3$(H_2O)$_2$], calculated: C, 31.59%; H, 1.41%. Found: C, 31.37%; H, 1.59%. For [Pr(tfnb)$_3$(H_2O)$_2$], calculated: C, 52.04%; H, 2.60%. Found: C, 51.89%; H, 2.84% [16].

2.6. Synthesis of SBA-15 mesoporous material covalently bonded with [Ln(hfth)$_3$phen] ternary complex [denoted as Ln(hfth)$_3$phen–S15, Ln = Er, Nd, Yb, Sm, Pr]

Phen–S15 was soaked in an excess of [Ln(hfth)$_3$(H_2O)$_2$] ethanol solution [12 equiv. of [Ln(hfth)$_3$(H_2O)$_2$] per phen moiety] under stirring. The mixture was heated under reflux for 6 h and was recovered by filtration. The excess reactants (such as [Ln(hfth)$_3$(H_2O)$_2$] complexes) in the Ln(hfth)$_3$phen–S15 were removed by Soxhlet extraction with acetone heated under reflux for 10 h. The resulting samples were dried at 80 °C under vacuum for 12 h.

2.7. Synthesis of SBA-15 mesoporous material covalently bonded with [Pr(tfnb)$_3$phen] ternary complex [denoted as Pr(tfnb)$_3$phen–S15]

The synthesis method for Pr(tfnb)$_3$phen–S15 was similar to that for Ln(hfth)$_3$phen–S15 except that [Ln(hfth)$_3$(H_2O)$_2$] was replaced by [Pr(tfnb)$_3$(H_2O)$_2$].

2.8. Characterization

The CH elemental analyses were carried out on a VarioEL analyzer. Small-angle X-ray diffraction (XRD) patterns were recorded with a Rigaku-Dmax 2500 diffractometer using Cu Kα radiation (40 kV, 200 mA) at a step width of 0.01°. Nitrogen (N_2) adsorption/desorption isotherms were measured by using a Nova 1000 analyzer with nitrogen. The samples were outgassed for 4 h at 120 °C before the measurements. Surface areas were calculated by the Brunauer–Emmett–Teller (BET) method and pore sizes by the Barrett–Joyner–Halenda (BJH) methods. The structures of the lanthanide-complex-functionalized mesoporous materials were characterized by transmission electron microscopy (TEM). All of the samples for the TEM characterization were prepared by directly transferring the suspended products to the standard copper grid coated with an amorphous carbon film. TEM was carried out on a JEOL-JEM-2010 at 200 kV. The excitation and emission spectra of

Table 1
Structural parameters of phen–S15, Ln(hfth)$_3$phen–S15 (Ln = Er, Nd, Yb, Sm) and Pr(tfnb)$_3$phen–S15 materials

Sample	d_{100} (nm)	a (nm)	S_{BET} ($m^2\,g^{-1}$)	V ($cm^3\,g^{-1}$)	D (nm)	h_w (nm)
phen–S15	11.04	12.75	938.7	1.43	6.46	6.29
Er(hfth)$_3$phen–S15	11.47	13.24	778.4	1.22	5.74	7.50
Nd(hfth)$_3$phen–S15	11.45	13.22	732.6	1.17	5.75	7.47
Yb(hfth)$_3$phen–S15	11.33	13.08	720.5	1.17	5.70	7.38
Sm(hfth)$_3$phen–S15	11.18	12.91	766.5	1.22	5.74	7.17
Pr(tfnb)$_3$phen–S15	11.18	12.91	784.7	1.24	5.73	7.18

d_{100} is the $d(1\,0\,0)$ spacing, a the cell parameter ($a = 2d_{100}/\sqrt{3}$), S_{BET} the BET surface area, V the total pore volume, D the average pore diameter, and h_w the wall thickness, calculated by $a - D$.

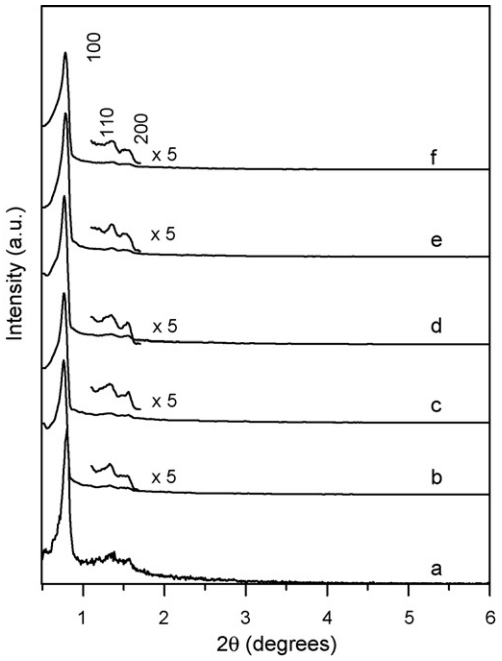

Fig. 1. XRD patterns of surfactant-extracted phen–S15 (a), Er(hfth)$_3$phen–S15 (b), Nd(hfth)$_3$phen–S15 (c), Yb(hfth)$_3$phen–S15 (d), Sm(hfth)$_3$phen–S15 (e), and Pr(tfnb)$_3$phen–S15 (f).

the solid-state samples were measured with an Edinburgh Analytical Instruments FLS920 equipped with the laser diode (LD) from the PicoQuant Company as the light source. The time-resolved measurements, for Nd(hfth)$_3$phen–S15 and Yb(hfth)$_3$phen–S15 were done on an Edinburgh Instruments FLS920, for Er(hfth)$_3$phen–S15, Sm(hfth)$_3$phen–S15 and Pr(tfnb)$_3$phen–S15 were done by using the third harmonic (355 nm) of a Spectra-physics Nd:YAG laser with a 5 ns pulse width and 5 mJ of energy per pulse as the source, and the NIR emission lines were dispersed by the emission monochromator of the HORIBA Jobin Yvon FluoroLog-3 equipped with liquid-nitrogen-cooled R5509-72 PMT, and the data were analysed with a LeCroy WaveRunner 6100 1 GHz Oscilloscope.

3. Results and discussion

3.1. Powder XRD

The power XRD analyses performed on phen–S15, Ln(hfth)$_3$phen–S15 (Ln = Er, Nd, Yb, Sm), and Pr(tfnb)$_3$phen–S15 are compared in Fig. 1, which show three Bragg peaks in the 2θ range of 0.8–2°. The prominent peak should be indexed as (1 0 0) diffraction peak and the other two as (1 1 0) and (2 0 0) diffraction peaks, which is characteristic of two-dimensional hexagonal (*p*6*mm*) structure of SBA-15 material. The corresponding unit cell parameters *a* of phen–S15, Ln(hfth)$_3$phen–S15 (Ln = Er, Nd, Yb, Sm), and Pr(tfnb)$_3$phen–S15 are 12.75, 13.24, 13.22, 13.08, 12.91, and 12.91 nm, respectively (see Table 1). Compared with the XRD pattern of the parent phen–S15 material, the d_{100} spacing values of the Ln(hfth)$_3$phen–S15 and Pr(tfnb)$_3$phen–S15 are similar to that of the phen–S15 material, which indicates that the framework hexagonal ordering has been preserved well upon the introduction of [Ln(hfth)$_3$(H$_2$O)$_2$] and [Pr(tfnb)$_3$(H$_2$O)$_2$] complexes, respectively [18]. In addition, it can be observed that the lanthanide-complex-functionalized materials show decrease in diffraction intensity in comparison with the parent phen–S15. This is probably due to the presence of [Ln(hfth)$_3$] and [Pr(tfnb)$_3$] moieties inside the pores of Ln(hfth)$_3$phen–S15 and Pr(tfnb)$_3$phen–S15 materials, respectively, which results in the decrease of the mesophase order [19]. It was reported that the introduction of guest into the pores leads to an increased phase cancellation between the guest moiety from the wall and the pore regions and accordingly to reduced scattering intensities for the Bragg reflections [20].

3.2. TEM

The TEM images in Fig. 2 show the preservation of highly ordered hexagonal mesostructure in the Ln(hfth)$_3$phen–S15 and Pr(tfnb)$_3$phen–S15 materials, which is in full agreement with the results of the XRD patterns. As shown in the figure, for all the lanthanide-complex-functionalized mesoporous materials there are regular hexagonal array of uniform channels characteristic of mesoporous SBA-15 material, which indicates that the mesostructure of the Ln(hfth)$_3$phen–S15 and Pr(tfnb)$_3$phen–S15 materials can be substantially conserved after the complexation process. The distances between the centers of the mesopore in Ln(hfth)$_3$phen–S15 and Pr(tfnb)$_3$phen–S15 materials are similar and estimated to be around 13 nm, which is in good agreement with the value determined from the corresponding XRD data (see Table 1).

3.3. Nitrogen adsorption/desorption

Nitrogen adsorption/desorption measurements were conducted to investigate the pore structures further. Fig. 3 shows the nitrogen adsorption/desorption isotherms for the surfactant-extracted phen–S15, Ln(hfth)$_3$phen–S15, and Pr(tfnb)$_3$phen–S15 materials. They all show typical type IV isotherm with a H1 type hysteresis loop at high relative pressure similar to that of the parent phen–S15 material, characteristic of ordered mesoporous materials according to the IUPAC classification [21]. By using BET and BJH methods, the specific area and the pore size have been calculated, which as well as the pore volume are shown in Table 1. With the linking of lanthanide complexes onto the parent material phen–S15, the pore sizes are decreased from 6.46 to 5.74, 5.75, 5.70, 5.74, and 5.73 nm for Er(hfth)$_3$phen–S15, Nd(hfth)$_3$phen–S15, Yb(hfth)$_3$phen–S15, Sm(hfth)$_3$phen–S15, and Pr(tfnb)$_3$phen–S15, respectively, and the BET surface area and pore volume correspondingly decrease as well. This is consistent with the presence of anchored [Ln(hfth)$_3$] and [Pr(tfnb)$_3$] moieties in the Ln(hfth)$_3$phen–S15 and Pr(tfnb)$_3$phen–S15 mesoporous channels. The phenomenon originates from the dispersion of the lanthanide complexes on the surface of the parent phen–S15 material, since these covalently complexes that dispersed inside the channel will always enhance the roughness of the pore surfaces and then make the surface area, pore volume, and pore size of these materials much smaller than those of the parent phen–S15 material [22,23].

3.4. Luminescent studies

Fig. 4 shows the excitation and emission spectra for the Er(hfth)$_3$phen–S15 material. The excitation spectrum, monitoring the strongest emission band of the Er^{3+} ion, presents a large broad band between 250 and 425 nm, which is attributed to the light absorption of the β-diketonate and the modified Phen-Si ligands. Under excitation at 397 nm, the emission spectrum displays an emission band centered at 1540 nm, and it should be attributed to the transition of $^4I_{13/2} \rightarrow {}^4I_{15/2}$ [24]. As shown in Scheme 1, while emission from a number of excited states from Er^{3+} ion is feasible, only emission from the $^4I_{13/2}$ state is observed, which suggests that an efficient non-radiative decay mechanism exists from these states to the $^4I_{13/2}$ state. The Er-containing materials are espe-

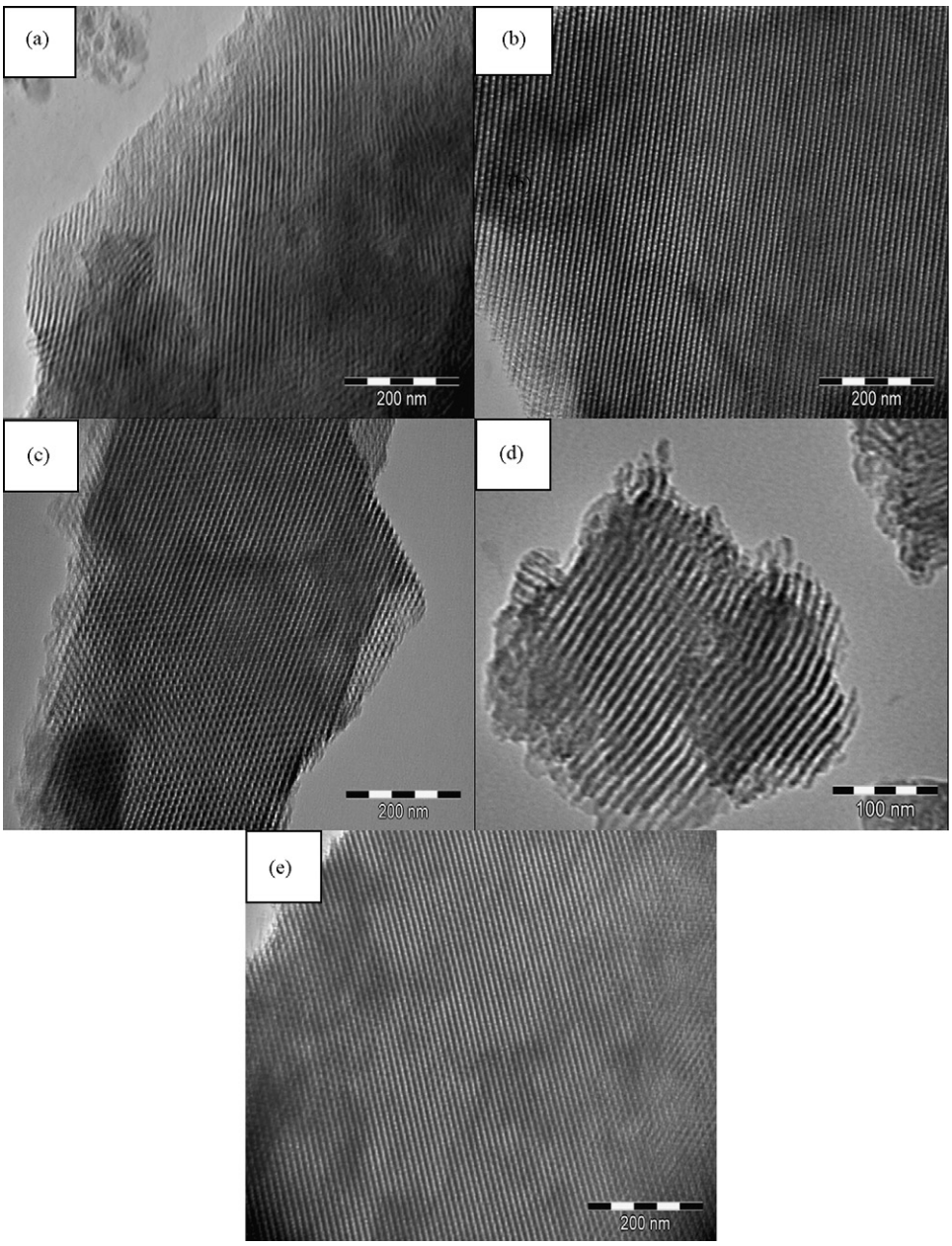

Fig. 2. TEM images of Er(hfth)$_3$phen–S15 (a), Nd(hfth)$_3$phen–S15 (b), Yb(hfth)$_3$phen–S15 (c), Sm(hfth)$_3$phen–S15 (d), and Pr(tfnb)$_3$phen–S15 (e).

cially interesting for application in optical amplification, because the transition around 1540 nm is in the right position of the third telecommunication window. In addition, a broad emission band is desirable to enable a wide gain bandwidth for optical amplification [24]. For the Er(hfth)$_3$phen–S15 material, the full width at half maximum (FWHM) of the $^4I_{13/2} \rightarrow {}^4I_{15/2}$ transition is 78 nm, and such a broad band enables a wide gain bandwidth for optical amplifier.

The fluorescence spectra of Nd(hfth)$_3$phen–S15 material are shown in Fig. 5. The broad band shown in the excitation spectrum is also assigned to the absorption of the hfth and the modified Phen-Si ligands. After ligand-mediated excitation at 368 nm, the emission spectrum displays three sets of emission bands characteristic for the Nd^{3+} ion in the NIR-region: an emission band at 854–942 nm ($^4F_{3/2} \rightarrow {}^4I_{9/2}$), a strong emission band at 1020–1130 nm ($^4F_{3/2} \rightarrow {}^4I_{11/2}$), and a weak band at about 1290–1408 nm ($^4F_{3/2} \rightarrow {}^4I_{13/2}$) [25]. Among the three emission bands of the Nd(hfth)$_3$phen–S15 material, the intensity of the transition at 1065 nm is the strongest, which has potential application in laser system, such as in the application of Nd/YAG laser. The emission band at 1335 nm of the material offers the opportunity to develop new materials, which are suitable for the optical amplifiers operating at 1.3 μm [25].

Yb^{3+} ion is a special case among the NIR-emitting lanthanide ions, because it has only one excited 4f state, namely the $^2F_{5/2}$ level, whose energy level is 10,200 cm^{-1} above the ground state (Scheme 1). The excitation and emission spectra of the Yb(hfth)$_3$phen–S15 material are displayed in Fig. 6. Upon excitation at the ligands absorption band (λ_{ex} = 397 nm), the emission spectrum of Yb(hfth)$_3$phen–S15 material was obtained. The emission band is split into three components, the strongest of which is centred at 980 nm, and two weaker components can also be observed, one at 1012 nm and another one at 1032 nm, assigned to the $^2F_{5/2} \rightarrow {}^2F_{7/2}$ transition of the Yb^{3+} ion [26]. Similar splitting has been reported in the previously literature [26,27]. This may be

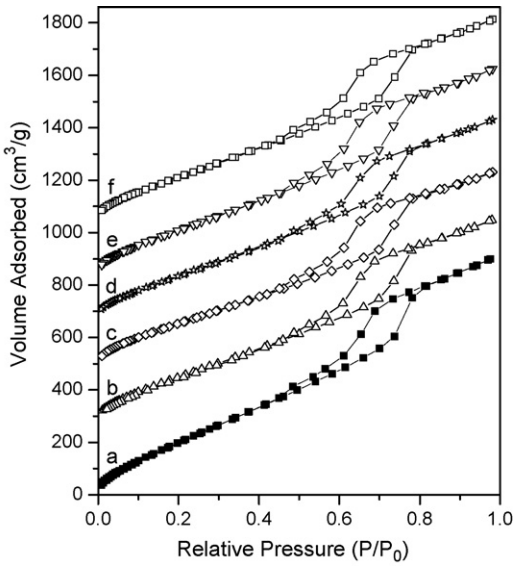

Fig. 3. N_2 adsorption/desorption isotherms of phen–S15 (a), Er(hfth)$_3$phen–S15 (b), Nd(hfth)$_3$phen–S15 (c), Yb(hfth)$_3$phen–S15 (d), Sm(hfth)$_3$phen–S15 (e), and Pr(tfnb)$_3$phen–S15 (f).

the splitting of the energy levels of Yb^{3+} ion as a consequence of ligand field effects [28]. The Yb^{3+} ion plays an important role in optical amplifiers and laser emission, which is often used as codopants in lasers and optical amplifiers because of its relatively broad absorption (with a relatively high absorption coefficient) and emission band at 980 nm and the possibility of transferring this energy to other lanthanide ions, like Pr^{3+} [29], Er^{3+} [30], and Tm^{3+} [31].

With respect to NIR-luminescent materials containing the lanthanide complexes, most researches are limited to the Er^{3+}, Nd^{3+}, and Yb^{3+} complexes [26,27,32]. Yet, the development and exploitation of the NIR-luminescent materials containing Sm or Pr complex lags a way behind that of the lanthanide complexes mentioned above. For Sm(hfth)$_3$phen–S15, the excitation and emission spectra was displayed in Fig. 7. The excitation spectrum monitored at 948 nm is composed of a broad band in the ultraviolet/visible spectral range, which is due to the absorption of the ligands. By using the excitation wavelength of 370 nm, the narrow bands are observed in the emission spectrum, which can be assigned to the

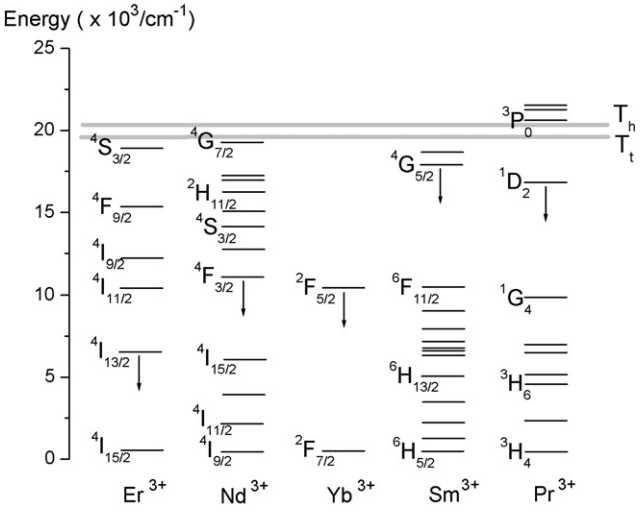

Scheme 1. Simplified energy diagram showing the lowest Ln^{3+} ion excited states and the triplet states of the Hhfth (T_h) and Htfnb (T_t) ligands.

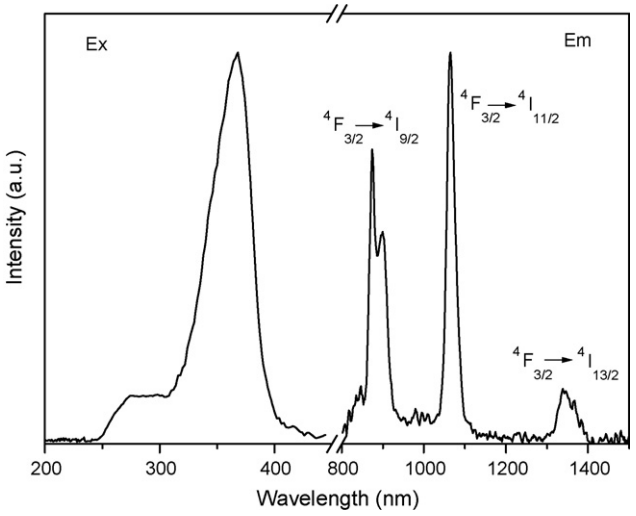

Fig. 5. Excitation (λ_{em} = 1065 nm) and emission (λ_{ex} = 368 nm) spectra for the Nd(hfth)$_3$phen–S15 material.

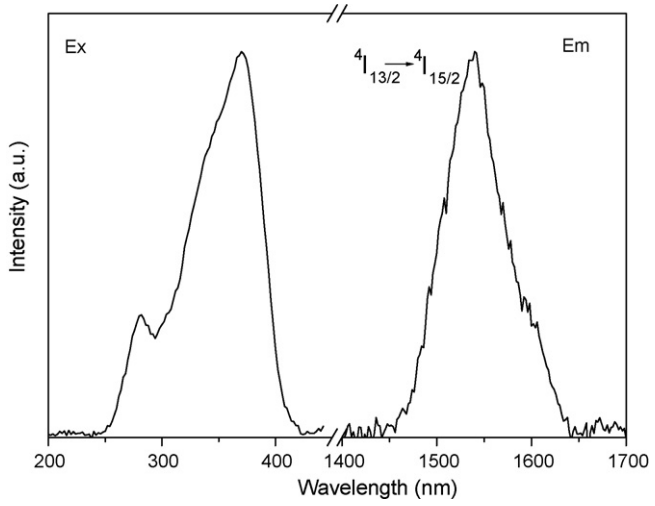

Fig. 4. Excitation (λ_{em} = 1540 nm) and emission (λ_{ex} = 397 nm) spectra for the Er(hfth)$_3$phen–S15 material.

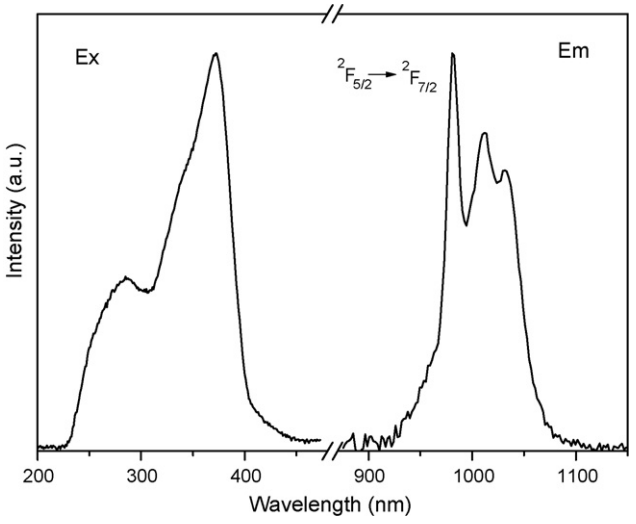

Fig. 6. Excitation (λ_{em} = 980 nm) and emission (λ_{ex} = 397 nm) spectra for the Yb(hfth)$_3$phen–S15 material.

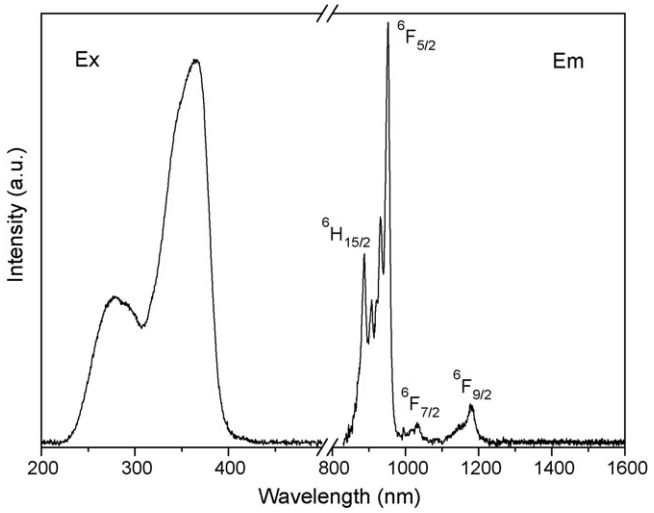

Fig. 7. Excitation (λ_{em} = 948 nm) and emission (λ_{ex} = 370 nm) spectra for the Sm(hfth)$_3$phen–S15 material. All the transitions start from the $^4G_{5/2}$ level.

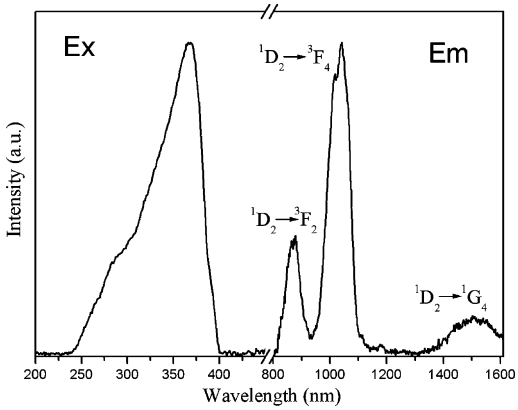

Fig. 8. Excitation (λ_{em} = 1038 nm) and emission (λ_{ex} = 365 nm) spectra for the Pr(tfnb)$_3$phen–S15 material.

transitions between the $^4G_{5/2}$ excited state and the $^6H_{15/2}$ and ^6F_J levels (J = 5/2–11/2) [26]. Among these transitions, the transition of $^4G_{5/2} \rightarrow {}^6F_{5/2}$ at 951 nm is the strongest.

The luminescence of Pr^{3+} ion is more complicated compared with that of the other lanthanide ions, such as Er^{3+}, Nd^{3+}, and Yb^{3+} ions, since Pr^{3+} ion can show emission lines originating from three different levels ($^3P_0$, $^1D_2$ and $^1G_4$) [33]. Transitions from the $^1D_2$ level are more probable than transitions from the $^3P_0$ level, since radiative transitions are more likely to occur when energy gaps are larger [34]. The $^1D_2$ level exhibits the largest energy gap of 6950 cm^{-1} (3860 cm^{-1} for $^3P_0 \rightarrow {}^1D_2$) to the next lower lying level $^1G_4$. For the Hhfth ligand, the triplet state is 20,400 cm^{-1}, which is close to the $^3P_0$ level (20,700 cm^{-1}, see Scheme 1) of Pr^{3+} ion. The small energy gap then would permit energy backtransfer, that is $^3P_0 \rightarrow L_T$ (L_T is the triplet ligand state). As a result, the $^3P_0$-luminescence of the Pr^{3+} ion is almost completely quenched by the energy backtransfer upon excitation of the ligands absorption [33]. In addition, the energy gap between the triplet state of Hhfth and $^1D_2$ level is large (~3600 cm^{-1}) and consequently the energy transfer rate is low. Therefore, the Pr(hfth)$_3$phen–S15 material was not further studied due to its poor luminescent property.

Recently, there has been growing interest in the design and synthesis of efficient NIR luminescence materials based on lanthanide complexes. Most researches have been focused on sensitizers with a triplet state matching the receiving lanthanide ion energy level so that efficient energy transfer can be obtained. For β-diketone ligands, they all bear two carbonyl groups that are separated by one carbon atom. The substituent on the carbonyl function, which has an important influence on the position of the energy levels of the ligand (singlet and triplet states), can be an alkyl group, a fluorinated alkyl group, an aromatic or a heteroaromatic group [9]. To match well with the $^1D_2$ level of Pr^{3+} ion, the Htfnb ligand, whose triplet state lies at 19,700 cm^{-1} [35], was synthesized as the main sensitizer for the NIR luminescence of Pr^{3+} ion. Fig. 8 shows the excitation and emission spectra of Pr(tfnb)$_3$phen–S15 material. The excitation spectrum is dominated by a broad band centered at 365 nm, which is due to the absorption of the tfnb and Phen-Si ligands. After ligand-mediated excitation at 365 nm, the emission spectrum clearly shows three bands at 878, 1042, and 1502 nm, which are attributed to the f–f transitions of $^1D_2 \rightarrow {}^3F_2$, $^1D_2 \rightarrow {}^3F_4$, and $^1D_2 \rightarrow {}^1G_4$, respectively [36]. In addition, the absence of the emission band at about 1320 nm assigned to the transition of $^1G_4 \rightarrow {}^3H_5$ indicates that the non-radiative process with phonon assistance dominates the relaxation of $^1G_4$ manifold energy levels. Therefore, the emitting band at 1040 nm is not from the $^1G_4$ level, that is, it is assigned to $^1D_2 \rightarrow {}^3F_4$ transition, not $^1G_4 \rightarrow {}^3H_4$ transition [33–36].

Time-resolved luminescence experiments were carried out on these NIR-luminescent mesoporous materials by monitoring around the strongest emission lines (at 1540 nm for Er(hfth)$_3$phen–S15, 1064 nm for Nd(hfth)$_3$phen–S15, 980 nm for Yb(hfth)$_3$phen–S15, 948 nm for Sm(hfth)$_3$phen–S15, and 1038 nm for Pr(tfnb)$_3$phen–S15). The decay curves of Er(hfth)$_3$phen–S15,

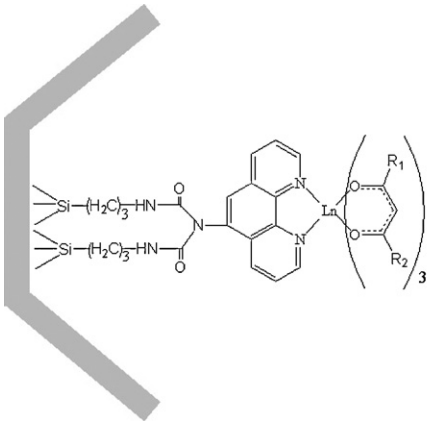

Ln	Er, Nd, Yb, Sm	Pr
R_1		
R_2	C_3F_7	CF_3

Scheme 2. Proposed structure of the Ln(hfth)$_3$phen–S15 (Ln = Er, Nd, Yb, Sm) and Pr(tfnb)$_3$phen–S15 mesoporous materials.

Nd(hfth)$_3$phen–S15, and Yb(hfth)$_3$phen–S15 fit single-exponential component well, and the corresponding lifetimes of the $^4I_{13/2} \rightarrow {}^4I_{15/2}$, $^4F_{3/2} \rightarrow {}^4I_{11/2}$, and $^2F_{5/2} \rightarrow {}^2F_{7/2}$ transitions are 1.22, 15.6, and 12.3 μs, respectively. The decay curves for Sm(hfth)$_3$phen–S15 and Pr(tfnb)$_3$phen–S15 can be fitted by double-exponential functions. The lifetimes of $^4G_{5/2} \rightarrow {}^6F_{5/2}$ transition of Sm(hfth)$_3$phen–S15 are 11.4 μs (38.55%) and 68.1 μs (61.45%). The lifetimes of $^1D_2 \rightarrow {}^3F_4$ transition of Pr(tfnb)$_3$phen–S15 are 12.5 ns (75.25%) and 62.9 ns (24.75%).

In order to obtain stable lanthanide materials with better optical properties, an important issue in the design of NIR-emitting lanthanide materials is to avoid water molecules from binding to the lanthanide ion in the first coordination sphere. Water molecules are very efficient quenchers for NIR luminescence, especially when present in the first coordination sphere [37]. In the mesoporous materials obtained above, the Phen-Si acts as a bidentate ligand and expels two water molecules from the first coordination sphere of the introduced [Ln(hfth)$_3$(H$_2$O)$_2$] and [Pr(tfnb)$_3$(H$_2$O)$_2$] complexes (Ln = Er, Nd, Yb, Sm). In this way, [Ln(hfth)$_3$phen] and [Pr(tfnb)$_3$phen] complexes are suggested to form and attach to the SBA-15 mesoporous material, respectively (Scheme 2) [38].

Because no absorption of the lanthanide ions occurs at the corresponding excitation wavelengths, the observed NIR luminescence can only arise from sensitization of the lanthanide ions by the organic ligands moiety. It is reasonable to conclude that the intramolecular energy transfer does happen between the organic ligands and the lanthanide ions in these NIR-luminescent mesoporous materials. This is the further evidence that ternary complexes [Ln(hfth)$_3$phen] and [Pr(tfnb)$_3$phen] are formed and covalently bonded to the mesoporous network in the Ln(hfth)$_3$phen–S15 and Pr(tfnb)$_3$phen–S15 materials, respectively.

4. Conclusions

New NIR-luminescent mesoporous materials Ln(hfth)$_3$phen –S15 and Pr(tfnb)$_3$phen–S15 were successfully prepared by linking ternary lanthanide (Er^{3+}, Nd^{3+}, Yb^{3+}, Sm^{3+}, Pr^{3+}) complexes to the ordered mesoporous SBA-15 through the functionalized Phen-Si ligand. All the derivative materials Ln(hfth)$_3$phen–S15 and Pr(tfnb)$_3$phen–S15 preserve their mesoscopically ordered structures and show highly uniform pore size distributions. Upon excitation at the absorption of the organic ligands, all these materials display the characteristic NIR luminescence of the corresponding lanthanide ions, which shows that the β-diketonate ligands (hfth or tfnb) and modified Phen-Si ligands can shield the lanthanide ions well from their surroundings and efficiently transfer the absorbed energy to the lanthanide ions. These NIR-luminescent mesoporous materials could have potential applications in optical amplifiers (operating at 1.3 or 1.5 μm) and laser systems. Of importance here is the observation of efficiently NIR luminescence in mesoporous SBA-15 materials covalently linked with Sm and Pr complexes.

Acknowledgments

The authors are grateful to the financial aid from the National Natural Science Foundation of China (Grant Nos. 20490210, 206301040, 20602035 and 20771099) and the MOST of China (Grant Nos. 2006CB601103 and 2006DFA42610). We are grateful to Dr. E. Ma of the Fujian Institute of Research on the Structure of Matter, Chinese Academy of Sciences for assistance with the fluorescence measurements.

References

[1] V. Bekiari, P. Lianos, Adv. Mater. 12 (2000) 1603.
[2] Z. Hong, C. Liang, R. Li, W. Li, D. Zhao, D. Fan, D. Wang, B. Chu, F. Zang, L.-S. Hong, S.-T. Lee, Adv. Mater. 16 (2001) 1241.
[3] S. Quici, M. Cavazzini, G. Marzanni, G. Accorsi, N. Armaroli, B. Ventura, F. Barigelletti, Inorg. Chem. 44 (2005) 529.
[4] L.H. Slooff, A. Polman, M.P.O. Wolbers, F.C.J.M. van Veggel, D.N. Reinhoudt, J.W. Hofstraat, J. Appl. Phys. 83 (1998) 497.
[5] K. Kuriki, Y. Koike, Y. Okamoto, Chem. Rev. 102 (2002) 2347.
[6] G.M. Davies, R.J. Aarons, G.R. Motson, J.C. Jeffery, H. Adams, S. Faulkner, M.D. Ward, J. Chem. Soc. Dalton Trans. (2004) 1136.
[7] M.H.V. Werts, J.W. Hofstraat, F.A.J. Geurts, J.W. Verhoeven, Chem. Phys. Lett. 276 (1997) 196.
[8] G.F. de Sa, O.L. Malta, C.D. Donega, A.M. Simas, R.L. Longo, P.A. Santa-Cruz, E.F. da Silva, Coord. Chem. Rev. 196 (2000) 165.
[9] K. Binnemans, in: K.A. Gschneidner Jr., J.-C.G. Bünzli, V.K. Pecharsky (Eds.), Handbook on the Physics and Chemistry of Rare Earths, vol. 35, Elsevier, Amsterdam, 2005, pp. 107–272 (chapter 225).
[10] L.N. Sun, J.B. Yu, G.L. Zheng, H.J. Zhang, Q.G. Meng, C.Y. Peng, L.S. Fu, F.Y. Liu, Y.N. Yu, Eur. J. Inorg. Chem. (2006) 3962.
[11] L.D. Carlos, R.A. Sá Ferreira, J.P. Rainho, V.Z. de Bermudez, Adv. Funct. Mater. 12 (2002) 819.
[12] C.T. Kresge, M.E. Leonowicz, W.J. Roth, J.C. Vartuli, J.S. Beck, Nature 359 (1992) 710.
[13] L.N. Sun, H.J. Zhang, C.Y. Peng, J.B. Yu, Q.G. Meng, L.S. Fu, F.Y. Liu, X.M. Guo, J. Phys. Chem. B 110 (2006) 7249.
[14] J.-P. Lecomte, A.K.D. Mesmaeker, M. Demeunynck, J. Lhomme, J. Chem. Soc., Faraday Trans. 89 (1993) 3261.
[15] H.R. Li, J. Lin, H.J. Zhang, L.S. Fu, Q.G. Meng, S.B. Wang, Chem. Mater. 14 (2002) 3651.
[16] L.N. Sun, J.B. Yu, H.J. Zhang, Q.G. Meng, E. Ma, C.Y. Peng, K.Y. Yang, Microporous Mesoporous Mater. 98 (2007) 156.
[17] J.B. Yu, H.J. Zhang, L.S. Fu, R.P. Deng, L. Zhou, H.R. Li, F.Y. Liu, H.L. Fu, Inorg. Chem. Commun. 6 (2003) 852.
[18] A.B. Bourlinos, Th. Karakostas, D. Petridis, J. Phys. Chem. B 107 (2003) 920.
[19] C.Y. Peng, H.J. Zhang, J.B. Yu, Q.G. Meng, L.S. Fu, H.R. Li, L.N. Sun, X.M. Guo, J. Phys. Chem. B 109 (2005) 15278.
[20] M. Fröba, R. Köhn, G. Bouffaud, O. Richard, G. van Tendeloo, Chem. Mater. 11 (1999) 2858.
[21] D.H. Everett, Pure Appl. Chem. 31 (1972) 577.
[22] Z.Y. Wu, Q. Jiang, Y.M. Wang, H.J. Wang, L.B. Sun, L.Y. Shi, J.H. Xu, Y. Wang, Y. Chun, J.H. Zhu, Chem. Mater. 18 (2006) 4600.
[23] Y.M. Wang, Z.Y. Wu, L.Y. Shi, J.H. Zhu, Adv. Mater. 17 (2005) 323.
[24] R. Van Deun, P. Nockemann, C. Görller-Walrand, K. Binnemans, Chem. Phys. Lett. 397 (2004) 447.
[25] S.I. Klink, P.O. Alink, L. Grave, F.G.A. Peters, J.W. Hofstraat, F. Geurts, F.C.J.M. van Veggel, J. Chem. Soc., Perkin Trans. 2 (2001) 363.
[26] P. Lenaerts, K. Driesen, R. Van Deun, K. Binnemans, Chem. Mater. 17 (2005) 2148.
[27] L.N. Sun, H.J. Zhang, Q.G. Meng, F.Y. Liu, L.S. Fu, C.Y. Peng, J.B. Yu, G.L. Zheng, S.B. Wang, J. Phys. Chem. B 109 (2005) 6174.
[28] M.P.O. Wolbers, F.C.J.M. van Veggel, B.H.M. Snellink-Ruël, J.W. Hofstraat, F.A.J. Geurts, D.N. Reinhoudt, J. Chem. Soc., Perkin Trans. 2 (1998) 2141.
[29] Y. Ohishi, T. Kanamori, J. Temmyo, M. Wada, M. Yamada, M. Shimizu, K. Yoshino, H. Hanafusa, M. Horiguchi, S. Takahashi, Electron. Lett. 27 (1991) 1995.
[30] K. Hsu, C.M. Miller, J.T. Kringlebotn, E.M. Taylor, J. Townsend, D.N. Payne, Opt. Lett. 19 (1994) 886.
[31] G. Özen, J.P. Denis, P. Goldner, X. Wu, M. Genotelle, F. Pellé, Appl. Phys. Lett. 62 (1993) 928.
[32] S. Comby, J.-C.G. Bünzli, in: K.A. Gschneidner Jr., J.-C.G. Bünzli, V.K. Pecharsky (Eds.), Handbook on the Physics and Chemistry of Rare Earths, vol. 37, 2007, pp. 217–470 (chapter 235).
[33] A.I. Voloshin, N.M. Shavaleev, V.P. Kazakov, J. Lumin. 93 (2001) 199.
[34] A. Babai, A.V. Mudring, Chem. Mater. 17 (2005) 6230.
[35] J.B. Yu, H.J. Zhang, L. Zhou, R.P. Deng, J. Lumin., submitted for publication.
[36] Z.R. Hong, C.J. Liang, R.G. Li, F.X. Zang, D. Fan, W.L. Li, L.S. Hung, S.T. Lee, Appl. Phys. Lett. 79 (2001) 1942.
[37] R. Van Deun, P. Fias, K. Binnemans, C. Görller-Walrand, Phys. Chem. Chem. Phys. 5 (2003) 2754.
[38] P. Lenaerts, E. Ryckebosch, K. Driesen, R. Van Deun, P. Nockemann, C. Görller-Walrand, K. Binnemans, K. Driesen, J. Lumin. 114 (2005) 77.